Histone H3 as a redox switch in the nucleosome core particle: insights from molecular modeling †

Yasaman Karami, Roy González-Alemán, Mailys Duch, Yuya Qiu, Yani Kedjar, Emmanuelle Bignon

PCCP

ARTICLE TYPE

Cite this: DOI: 00.0000/xxxxxxxxxx

Histone H3 as a redox switch in the nucleosome core particle: insights from molecular modeling†

Yasaman Karami,[a‡] Roy González-Alemán,[b‡] Mailys Duch,[b] Yuya Qiu,[b] Yani Kedjar,[b] and Emmanuelle Bignon*[b]

Received Date
Accepted Date

DOI: 00.0000/xxxxxxxxxx

Histones post-translational modifications are major regulators of the chromatin dynamics. Understanding the structural signature of these marks in the nucleosome context is of major importance to unravel their mechanisms of action and open perspectives for the development of new therapies. In this work, we rely on multi-microseconds molecular dynamics simulations and advanced structural analysis to unravel the effect of two modifications of the histone H3: S-sulfenylation and S-nitrosylation. These oxidative modifications are known to target the cysteine 110 on the histone H3, but there was no data about their effect on the nucleosome dynamics. We show that in a nucleosome core particle, S-sulfenylation and S-nitrosylation exhibit different structural signatures, which could suggest that they play a different role in the regulation of the nucleosome dynamics. While S-sulfenylation destabilizes the dyad and could be involved in the nucleosome disassembly, S-nitrosylation mainly induces DNA flexibility at its entry/exit point, most probably favoring breathing/unwrapping phenomena. Our results highlight the fine tune link between the chemical nature of histone core post-translational modifications and their impact on such a large architecture as the nucleosome. They also provide new insights into the regulatory mechanisms of histone oxidative modifications, about which very little is known so far.

Introduction

In cells, DNA is tightly compacted by histone proteins to fit into the nucleus. At the first level of compaction, the so-called nucleosome, the double helix is wrapped onto an octamer of histone proteins[1] - see Figure 1-a. The histone core is constituted by two copies of four types of histones (H3, H4, H2A, and H2B), each of which exhibit a N-terminal disordered tail that protrude from the nucleosome core particle (NCP). Of note, H2A also has a disordered C-terminal tail.

DNA compaction is a dynamic phenomenon that is regulated by a plethora of epigenetic factors. Among them, post-translational modifications (PTMs) of histone proteins are crucial, and hundreds of them have been characterized to date[3]. They are known to regulate the dynamics of the nucleosome through highly complex mechanisms that remain ill-defined in many ways. Large

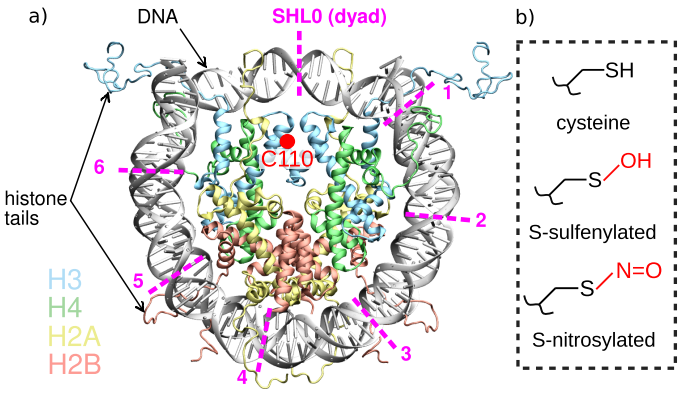

Fig. 1 a) Structure of a nucleosome core particle, composed of 145 DNA base pairs wrapped onto an octamer of histone proteins (H3 in blue, H4 in green, H2A in yellow, H2B in orange). Super helical locations are indicated in magenta with the dyad considered as SHL0. A red dot locates histone H3 cysteine 110, which can undergo oxidative modifications in the nucleosome. Adapted from Gillet et al[2]. b) Structure of a canonical cysteine (top) and its S-sulfenylated (center) and S-nitrosylated (bottom) derivatives.

[a] Université de Lorraine, CNRS, Inria, LORIA, F-54000 Nancy, France
[b] Université de Lorraine and CNRS, UMR 7019 LPCT, F-54000 Nancy, France; E-mail: emmanuelle.bignon@univ-lorraine.fr

† Electronic Supplementary Information (ESI) available: COMMA results for S-nitrosylation; Curves+ results; Full view of the nucleosome binding pockets; Descriptors of the binding pocket near H3C110; Hydrogen Bond mapping of DNA-histone interactions; DNA flexibility profile superimposition with previous results for S-sulfonylation; Table of histone core-DNA interaction prevalences. See DOI: 10.1039/cXCP00000x/

‡ These authors contributed equally to this work.

amounts of investigations have been focused on histone PTMs located on the histone tails, which can exhibit a direct effect on DNA/tails electrostatic interactions but can also influence the binding of partner proteins such as chromatin factors. The high complexity of the mechanisms of action associated with histone PTMs is further illustrated by their possible combinatorial effects (i.e. they could work as a 'histone code') and the fact that one amino acid can participate to opposite mechanisms depending on the nature of the modification it undergoes. For instance, H3K9 methylation is well known to promote chromatin compaction via its specific binding to the HP1 protein, while its acetylation participates to chromatin opening via direct perturbation of interactions with the DNA. Besides, the crosstalk between H3S10 phosphorylation and H3K9 acetylation has been highlighted as H3S10ph can block H3K9 methylation.

Modifications of amino acids on the histone core are, however, much less studied. It has been hypothesized that PTMs at the DNA/histone contact surface would promote either nucleosome disassembly when located near the dyad, or DNA unwrapping if positioned on the histone core lateral surface[4]. However, while numerous PTMs located away from the DNA-histone interface have been investigated by experimental means and while new PTMs are frequently discovered, the structural mechanisms of action of most of them remain to be described.

This is the case for oxidative PTMs, which target mainly cysteine residues of proteins, and are well known to regulate a large panel of proteins in cells and to be deregulated in many diseases. For instance, S-nitrosylation is well known to play a crucial role in many different signaling pathways, which are deregulated upon cancer onset and progression (e.g., proliferation, apoptosis)[5,6]. While it can result from the reaction between the cysteine's sulfur atom with nitric oxide or with low molecular weight -NO donor (e.g. GSNO), enzymes catalyzing protein (de-)nitrosylation are also known to target a wide range of proteins[7,8]. This is the case for insulin receptors, which are found to be nitrosylated by the recently identified SCAN enzyme[9]. S-sulfenylation is formed by reaction between the cysteine and reactive oxygen species (e.g. H_2O_2), and is also involved in the modulation of a plethora of proteins activity. It is well known as a major redox sensor influencing many signaling pathways[10] with, for instance, a role in the regulation of protein folding[11] and in vascular homeostasis maintenance[12]. Some irreversible oxidative PTMs such as S-sulfonylation are also markers of oxidative stress and can promote protein degradation[13,14].

In the nucleosome context, the histone H3 cysteine 110 is known to undergo different types of oxidative modifications[15,16], yet their role in the nucleosome dynamics regulation remains mostly unknown. However, experimental studies have shown that H3C110 S-gluthationylation promotes chromatin opening[17] and is linked to cell proliferation[18], while some of our recent computational works underlined the possible promotion of the nucleosome disassembly by S-sulfonylation[19]. While computational studies of the nucleosome dynamics and the effect of some mainstream PTMs have been released[20–25], there is a drastic lack of theoretical investigation concerning oxidative PTMs.

In this work, we investigate the effects of two oxidative modifications of histone proteins, H3C110 S-sulfenylation and S-nitrosylation (see Figure 1-b), on the structural and dynamic properties of a nucleosome core particle (NCP). We report in-depth structural analyses of 20 μs unbiased molecular dynamics (MD) simulations, highlighting dissimilar structural signatures of the two PTMs, which suggests a differential role in epigenetic regulation mechanisms.

Computational Methods

All MD simulations were performed with the AMBER20 suite of programs, while the VMD[26] and Pymol[27] software were used for visualization and figures rendering.

Systems setup

Starting systems were built from the crystal structure of the nucleosome core particle featuring an α-satellite DNA sequence and full histone tails (PDB ID 1KX5[28]). The only three missing residues (PEP) at the N-terminus of both H2B copies were reconstructed using VMD and visual inspection. Nitrosylation and sulfenylation were introduced on the first copy of H3C110 using the leap functionality of AMBER, which did not create any clash contact. The AMBER ff14SB force field[29] was used in combination with bsc1[30] and the CUFIX[31] corrections for non-bonded terms. Parameters for the sulfenylated cysteine were generated in house as described in previous work[19], while for nitrosylation they were taken from the literature[32].

Each modified system, i.e. with nitrosylation (named 1KX5+SNO) or with sulfenylation (named 1KX5+SOH), was placed into a TIP3P water box with a truncated octahedron shape using a buffer of 20Å. The addition of 434 Na^+ and 288 Cl^- ions ensured the neutrality and a salt concentration of 0.150M, resulting in systems of $\sim$427,000 atoms. A topology file with Hydrogen Mass Repartioning[33,34] was generated with the parmed program of AMBER to be used in the production run of the MD simulations.

Molecular dynamics protocol

The starting structures were first optimized in 4 steps with decreasing position restraints on the nucleosome core particle atoms from 20 kcal/mol to 5 kcal/mol. For each one of these 4 steps, a minimization run of 10,000 steps (with the steepest descent switched to conjugate gradient after 5,000 steps) was followed by a short equilibration run of 20 ps at 100K. This procedure allows the structure to be smoothly optimized in its environment. A final 10,000 steps minimization without restraint was then followed by 20 ps thermalization to increase the temperature to 300K and a 500 ps equilibration in NVT to equilibrate the solvent. The system was then relaxed in NPT during 100 ns before a 2 μs production run. The latter was performed using a 4 fs timestep allowed by the use of the HMR approach on the protein and DNA atoms[33,34]. Temperature and pressure were kept constant (300K, 1 bar) using the Langevin thermostat with a 2 ps^{-1} collision frequency and the Berendsen barostat with isotropic position scaling and a pressure relaxation time of 1 ps. A classical 8 Å cutoff was used for non-bonded terms, and long-range electrostatics were treated using the Particle Mesh Ewald approach[35]. Bonds involving hydrogen

were constrained using the SHAKE algorithm. For each system, five replicates were produced with random starting velocities, resulting in a total of 20 μs of sampling.
Control MD ensembles for the unmodified nucleosome core particle were taken from a previous work[19].

Structural analyses

The flexibility analysis was performed using a PCA-based python script that we successfully applied on other nucleosomal systems[19,36,37]. It uses the inverse distance between each pair of residues as internal coordinates, extracted directly from the MD trajectories. The eigenmodes and eigenvectors of the generated covariance matrix can be interpreted as the primary modes of motion and their amplitude. We can then determine how much each residue contributes to the system's overall flexibility by analyzing the per residue contribution to these motions.
DNA structural descriptors were computed using the Curves+ program[38]. We performed the analyses for all base pairs and all descriptors provided by Curves+. Only three sections were shown in the SI - see Figures S3-S5.
To track the progress of molecular interactions between DNA and the histone octamer, we utilized the ProLIF software[39]. The program's default geometrical definitions were applied to every ten frames of the trajectories. We observed several types of contacts between different moieties, including anionic, hydrogen bonding (acceptor and donor), Pi-Cation, Pi-Stacking, hydrophobic, and Vand-der-Waals. Two residues were considered interacting if, in more than 20% of the frames considered, any of the contacts mentioned above were detected between them. As this study focuses on re-organization of the histone core upon oxidation, we excluded the histone tails from the DNA-protein interaction analysis. It is however important to underline the fact that the disordered histone tails play a role in the interactions with the DNA in the NCP. Yet, the mapping of such interaction networks would require using enhanced sampling methods, which is out of the scope of the present study.
In order to determine if the MD ensembles exhibit binding sites close to H3C110, pockets were tracked along the MD ensembles using the MDPocket software[40]. It was also interesting to scrutinize to what extent histone H3 sulfenylation and nitrosylation would influence binding sites on the nucleosome core particle architecture, because these two modifications are thought to be precursors for H3C110 S-glutathionylation by reaction with glutathione (a pseudo-tripeptide see Figure S1), but could also modulate binding sites on the NCP for partner proteins. Analyses were performed on the control system (1KX5) and on the modified ones (1KX5+SNO and 1KX5+SOH), and specific descriptors (pocket volume, hydrophobicity...) were monitored for the pockets located near H3C110 and H3'C110.
The COMMA2 approach was used to extract the protein communication network[41]. First, a set of properties was extracted from every studied trajectory: communication propensity (variance of inter-residue distances), interaction strength, distances, dynamical correlation, and stability of the secondary structure. Then, we defined communication pathways: chains of residues that are not adjacent along the sequence, are linked by non-covalent interactions and communicate efficiently. These pathways form the protein communication network, in which nodes correspond to the residues of the protein and edges connect residues adjacent in a pathway. The communication blocks are then extracted as connected components of the graph (see[42] for detailed descriptions). Finally, we merged the results from all replicates of each system. Only the proteins were taken into account for the COMMA2 analysis.

Results and Discussion

S-sulfenylation destabilizes DNA-protein contacts at the dyad

In order to probe the effect of S-sulfenylation and S-nitrosylation on the DNA dynamical properties, we performed DNA flexibility analyses and used the Curves+ program to exhaustively capture its base-pair structural descriptors.

A major difference in the DNA flexibility profiles of the two modified systems is the destabilization of the dyad (around SHL0) by the S-sulfenylation - see Figure 2-a and c. This position of the DNA on the NCP is generally the most stable on the sequence, and drives DNA positioning onto the histone core. More specifically, this destabilization is observed for base pairs 68 to 83 and is more pronounced at SHL0.5 and SHL-0.5. This effect might result form the changes in the hydrogen bond networks involving histone residues in contact with these DNA locations, as described in the next section. S-sulfenylation also induces a destabilization of the DNA entry/exit point in an asymmetric manner. Indeed, an increase of the values is observed for the 15 terminal base-pairs with respect to the control. This trend results from the sampling of conformations featuring a breathing of the DNA gyre extremity, which can be scrutinized using two descriptors: a dihedral angle ϕ (SHL0-SHL-2-SHL5-SHL7) illustrating an opening in the plane of the NCP, and a θ angle (SHL0-SHL5-SHL7) which characterizes an out-of-plane deviation - see Figure 2-d. The distribution of these angles with respect to the control system highlights the sampling of conformations with a strongly pronounced opening upon S-sulfenylation, with ϕ values up to 80° ($\sim$34° in the control) and θ values up to 75 ° ($\sim$36° in the control) - see Figure 2-e. Noteworthy, a stabilization of the DNA is observed at SHL-3 and SHL4.5. In this region of the NCP, some interactions between DNA and histone core residues are strongly increased with respect to the control system, which might directly result from the perturbation of communication networks within the H3α2 helix - see more details below concerning communication pathways and hydrogen bond networks.

Interestingly, we previously reported a similar destabilization of DNA at the dyad upon S-sulfonylation (hyperoxidation) of histone H3 - see superimposition of the profiles in Figure S2. The destabilization of DNA at the dyad is a hallmark of remodeling events such as DNA sliding and NCP disassembly, which suggests that H3C110 oxidation by S-sulfenylation and its higher order oxidative derivatives might promote these phenomena.
Surprisingly, there is no perturbation of the dyad stability upon S-nitrosylation, highlighting dissimilar effects of the two modifications. Only a destabilization of the DNA entry/exit point is

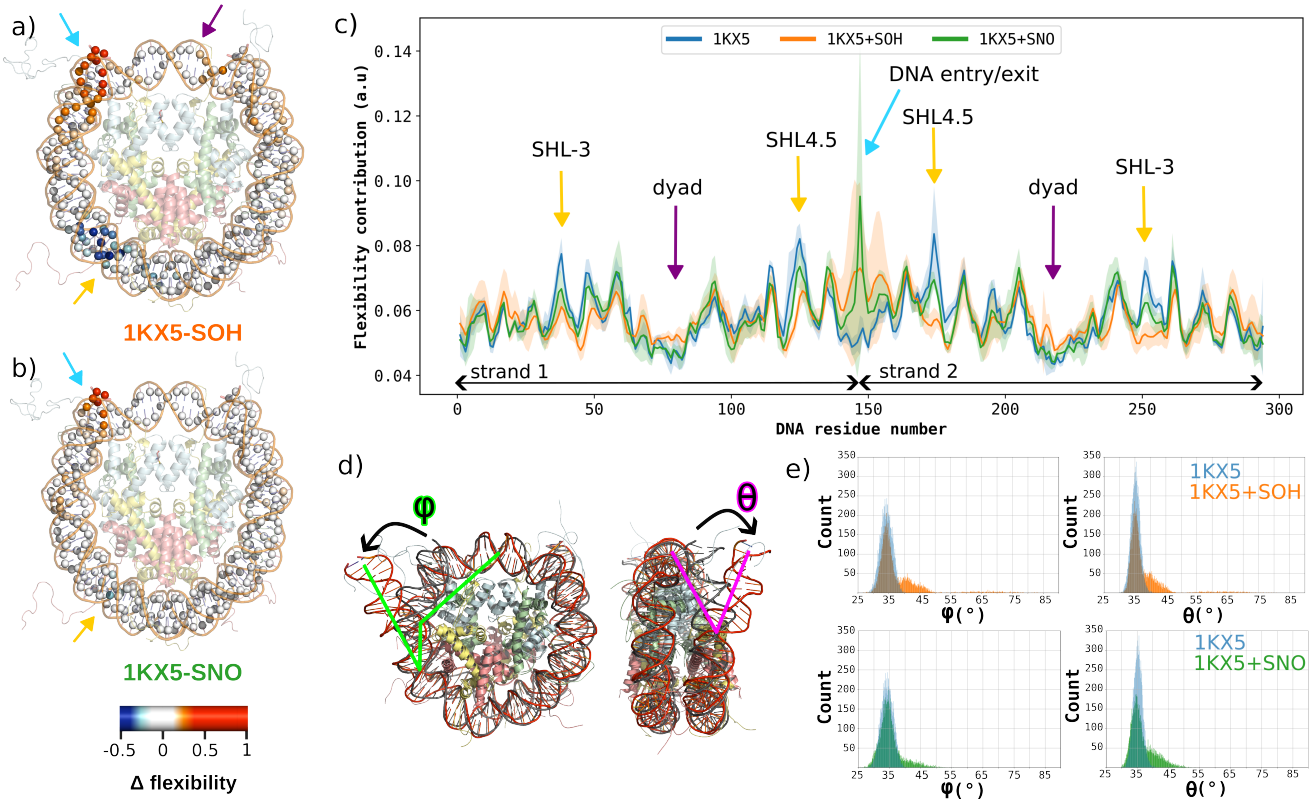

Fig. 2 a) Deviations of the DNA flexibility projected onto the NCP structure for the S-sulfenylated system (1KX5+SOH) with respect to the control system (1KX5), and b) for S-nitrosylation (1KX5+SNO) with respect to the control system. A decrease of flexibility is depicted in blue while and increase appears in red. Arrows highlight the regions showing the highest deviations, colored to match the ones in panel c. c) Profiles of per residue flexibility contribution for DNA in the S-sulfenylated (orange), S-nitrosylated (green) and control (blue) systems. Regions where deviations are observed and SHL positions (dyad = SHL0 and DNA entry/exit = SHL7 here) are labeled by colored arrows . d) Scheme of the ϕ dihedral angle and the *theta* angle that were monitored to characterize DNA breathing. e) Distribution of the *phi* and *theta* angles for control (in blue), S-sulfenylated (in orange, top) and S-nitrosylation (in green, bottom) systems.

observed on the 15 terminal base-pairs - see Figure 2-b and c. The asymmetry of DNA unwrapping has been observed experimentally and theoretically in the nucleosome[43,44], also suggesting rearrangements in the histone core that allow the formation of structural intermediates[45]. As for S-sulfenylation, conformations featuring an opening of the DNA extremity are observed, as showed by the distribution of ϕ and θ angles for this system. These angles do not reach peak values as high as for S-sulfenylation (max $\sim$55° for both ϕ and θ), yet their distribution highlights the non-negligible sampling of DNA breathing induced by the S-nitrosylation. Such DNA opening seems to be favored by a change in the dynamics of the histone H3 tail, as well as a rewiring of the DNA-histone core interactions at SHL6-7 as described below. The extensive monitoring of DNA structural descriptors with the Curves+ program did not reveal any significant deviation of the mean values from the control system, except for the DNA extremities as one could expect - see Figures S3-S5. Noteworthy though, standard deviations for several descriptors of base pairs near the dyad, especially around base pair 80 (SHL0.5), are larger with S-sulfenylation than in the control and S-nitrosylated systems (e.g. Shear, Stagger, Rise, Twist, Tip). This effect remains milder than what we observed in the case of S-sulfonylation, for which even larger deviations were observed at the dyad. Noteworthy, the flexibility profiles of the histone proteins do not show significant deviation from the control - see Figure S2.

Of note, the interaction between the histone tails and the DNA can also influence the DNA dynamics[46]. While in the simulations with S-sulfenylation there is not contact between the H3/H3' tails and DNA at the dyad, we can observe this type of interaction involving the H3' tail in the control and S-nitrosylated systems, but also in the S-sulfonylated one (calculated from MD simulations of our previous work[19]) - see Figure S6. Thus, the increase in flexibility of the DNA helix at the dyad is not correlated to the difference of H3 tails-DNA contacts in this region, as S-sulfenylation and S-sulfonylation both provoke an increase of DNA flexibility at the dyad but show dissimilar H3'-DNA interaction patterns.
The H4/H4' and H2A/H2A' conformations are not highly perturbed by the presence of any modification (S-sulfenylation, S-nitrosylation or S-sulfonylation) - see Figures S7 and S8. However, the H2B/H2B' tails conformations exhibit non-negligible fluctuations upon H3 S-sulenylation and S-nitrosylation, which could have a role in the stiffening of the DNA in the SHL-3/SHL4.5 regions which is especially marked for S-sulfenylated systems -see Figure S9.

These results reveal that, analogously to lysine acetylation vs

methylation, the chemical nature of the cysteine modification (oxidation to -SOH or $-SO_3^-$ vs nitrosylation to -SNO) might dictate its effect on DNA stability within the nucleosome. This suggests that PTMs near the dyad but not directly in contact with DNA might promote different signaling events depending on their chemical nature.

S-sulfenylation stabilizes the $(H3\text{-}H4)_2$ tetramer and induces allosteric effects

We recently showed how H3C110 hyperoxidation can induce a re-shaping of the histone core intrinsic architecture[19]. A similar protocol was used here to assess the effect of S-sulfenylation and S-nitrosylation on inter-histone communication pathways within the NCP. COMMA2 analyses were performed in order to characterize communication pathways, blocks and hubs (key-residues) within the histone core, revealing a dissimilar effect of the two oxidative modifications.

Upon S-sulfenylation, a large communication block unites the $(H3\text{-}H4)_2$ tetramer - see Figure 3. This denotes an increase of compactness on the upper part of the histone core with respect to the control system, which exhibits two to three blocks per dimer with the histone H3 α1 helix separated from the others. It is interesting to see that this modification induces a strengthening of the interactions in the H3-H3' bundle, namely between H3H113 and H3'D123 and its symmetric H3D123 and H3'H113, which generates communication pathways between the two H3-H4 dimers. S-sulfenylation also reduces the number of pathways transmitted along the entire H3α2 on which it is located. This was not expected as in our MD simulations the -SOH moiety of the modified cysteine is rapidly trapped in a hydrogen bond with the backbone carbonyl of the vicinal H3D106, which is similar to what happens in the control system (i.e. with -SH) - see Figure S10. Besides, we observe an increase of the pathways mediated by the H3'α2 helix at its lower end, with larger hubs at positions A87, M89 and A90. This denotes a possible allosteric modulation of DNA-protein interactions induced by S-sulfenylation, as supported by the analysis of the contact network - see next section. Noteworthy, it does not provoke any significant change in the communication pathways within the H2A-H2B dimers, suggesting that the effect of the modification is limited to the $(H3\text{-}H4)_2$ tetramer.
S-nitrosylation induces much less pronounced changes of the histone core internal communication pathways - see Figure S10. The -SNO moiety does not form stable interactions with its surroundings. Interestingly, a slight reduction of the number of pathways in the H3α2 helix harboring the modification is observed as for S-sulfenylation, but in contrast the latter this effect is symmetrical and also affects the facing H3'α2 helix. Overall, the communication blocks distribution upon S-nitrosylation is highly similar to the control one, suggesting that this modification does not act as S-sulfenylation and may have a different role in nucleosome-related processes.

Noteworthy, S-sulfenylation perturbation of the communication pathways within the histone core differs from what was previously observed for another cysteine oxidative modification, the S-sulfonylation (cysteine hyperoxidation featuring a $-SO_3^-$ moiety)[19]. Indeed, the latter induces an increase of H2A-H2B compactness while preserving the per dimer organization in the $(H3\text{-}H4)_2$ tetramer. S-sulfonylation also provokes a much stronger loss of communication pathways around the modification site on H3α2, balanced by a marked increase of pathways in the rest of the histone core - see Figure S10. While S-sulfenylation and S-sulfonylation both destabilize the histone-DNA interactions at the dyad (see Figure S2), they reshape of communication blocks in a different manner, which results in dissimilar structural signatures that might translate into distinct roles in DNA compaction mechanisms. This could relate to the fact that S-sulfenylation is a reversible PTM involved in canonical redox signaling pathways, while S-sulfonylation is an irreversible end-product which induces drastic events such as protein degradation upon oxidative stress.

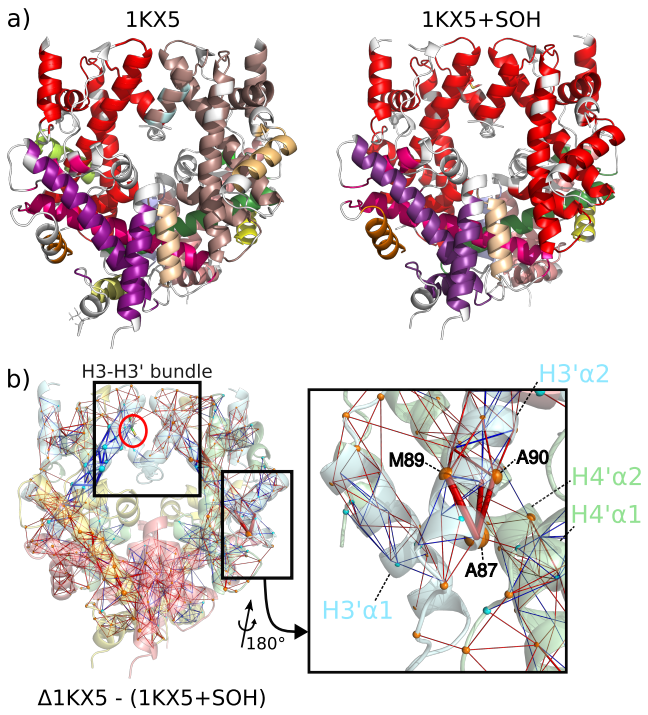

Fig. 3 a) Representation of the communication blocks within the histone core, for the control system (1KX5, left) and the S-sulfenylated system (1KX5+SOH, right). Each block is depicted in a different color. b) Projection of the changes in the communication pathways upon S-sulfenylation, showing strengthened pathways in the H3-H3' bundle and at the beginning of the H3'α2 helix. A zoom on the latter area shows the denser hubs (A87, M89, A90) and their connections with the surrounding residues.

Overall, S-sulfenylation mostly induces a strengthening of the communications in the $(H3\text{-}H4)_2$ tetramer while the effect of S-nitrosylation is focused on a local weakening of the pathways in the H3 and H3' α2 helices. These observations show how the nature of the cysteine modification could specifically modulate the histone core organization. While it is known that the modulation of histone dimers plasticity is strongly related to the nucleosome stability, the exact role of the intrinsic communication networks we describe remains to be investigated experimentally.

The DNA-histone contact network is reshaped by cysteine modifications

In the nucleosome core particle, an intense network of hydrogen bonds and salt bridges ensures the interaction between the DNA and the histone proteins, maintaining the overall architecture stability. We probed the effect of H3C110 S-sulfenylation and S-nitrosylation onto this network by exhaustively monitoring the DNA-histones interactions along the MD ensembles of the control and modified NCP. This allows to rationalize the perturbations of the DNA flexibility and the histone core communication networks above-described.

Scrutinizing the DNA-histone core contacts in the control system, we retrieve well-known interactions. Near the dyad, H3/H3'K64 strongly interact with dT239 (79%) and dT240 (23%)/dT92 (83%), while H4/H4'S47 interact with dT28 (56%)/dT81 (56%). To a lesser extent, interactions involving H3K115 (20% with dA220 and 38% with dG219) and H3'K115 (21% with dA73 and 41% with dG72), as well as H3K122 (25% dG72), are pinpointed. At the DNA entry/exit points, H3/H3'T339 interact with several nucleotides: 47% with dT144, 96% with dG145, 25% with dA230 / 45% with dT291, 97% with dG292, 23% with dA83. A very prevalent interaction involves H4K79 (100% dC249, 71% dG248) and its symmetric H4'K79 (100% dC102 and 73% dG101). H4K77 and H4'K77 contacts with dA41 and dA188 show a 39% and 53% prevalence, respectively. The H3/H3'K56 interaction with dC156/dC9 is also retrieved yet not strongly pronounced (22%/30%), while multiple contacts involving H3'Y41 (67% dT6, 36% dA7, 79% dA83, 88% dA84, 51% dT291, 65% dG292) are not observed in the H3 copy. Several canonical interactions of histone residues with the nucleobases themselves are also observed: H3R83 with base pairs 50-51, H3'R83 with base pairs 99-102, H4R45 with base pairs 69-70 and H4'R45 with base pairs 81-82, H2AR42 with base pairs 37-39 and H2A'R42 with base pairs 112-113, as well as H2AR77 with base pairs 19-20 and H2A'R77 with base pairs 132-133.
Our analysis also allows to pinpoint other very persistent DNA-histone interactions that involve non-polar or non-charged amino acids, providing a complete contact map between the histone core and the DNA gyres. Among the most important ones, there are several alanine residues: H3/H3'A47 (99% with dA230/dA83) and H2AA45/H2A'A45 (85%/90% with dA259/dA112). Few glycine residues are also involved in strong interactions with the DNA: H3/H3'G44 (95%/91% with dA230/dA83 and 94%/91% with dG229/dG82) and H4/H4'G48 (92%/95% with dT228/dT81). Finally, four valine residues show high interaction prevalences: H3/H3'46 (100% with dA230/dA83) and H3/H3'V116 (99% with dG71/dG218). Noteworthy, these interactions are all located between the SHL-1/SHL1 regions, near to the dyad. Hydrophobic residues might participate to the strong interaction network that makes the dyad the most strongly positioned part of the DNA in the NCP.

Upon oxidative modifications of H3C110, this interaction map is re-shaped - see Figure 4. For both S-sulfenylation and S-nitrosylation, we retrieve a decrease of prevalence for residues at the DNA entry/exit terminal base pairs that undergo an opening as above-described, especially pronounced for dG145 and dT144, dT155 and dC156 (base pairs 139 to 145). This seems to especially involve interactions with the residue H3T45, which interaction prevalence drastically drops upon both S-sulfenylation (-33% with dG145 and -19% with dT144) and S-nitrosylation (-30% with dG145 and -15% with dT144). Interestingly, S-sulfenylation induces larger shifts of the per residue DNA-histone interactions prevalence than S-nitrosylation. It provokes an overall loss of interaction between DNA and the histone core. Besides the DNA extremity, a significant decrease of interaction near SHL0.5 is also observed, involving dC216, dA214, and dC82 (base pairs 79-82) on the DNA side, and residues H3'P43, H4'R39 and H4'R45. This perturbation of DNA-histone contacts is most probably involved in the above-described DNA destabilization observed in this region. Interestingly, we previously showed that H4'R45 interactions with the DNA is also perturbed by S-sulfonylation, which can allow local sliding events of the DNA helix[19]. In the case of S-sulfenylation no DNA sliding was characterized, but these observations still highlight possible common mechanisms underlying S-sulfenylation and S-sulfonylation effect on the NCP dynamics.
Importantly, changes in DNA/histone core interactions might not be enough to explain the lower DNA flexibility characterized at SHL4.5 and SHL-3 (see Figure 2), as in this region both increases and decreases of the interaction prevalence are observed. Indeed, while there is an increase of the prevalence to interact with DNA for H4K77 (+20%), H4K79 (+14%), H2A'H31 (+22%) and H2A'R32 (+13%), H2AR20 and H4R78 exhibit fewer contacts with the nucleic acids (+10% and -29%, respectively). As the H2A and H2B tails protrude from the histone core near these SHL, their interactions with the DNA helix might also play an important role in the modulation of its flexibility.
The perturbation of the communication pathways along the H3 copies (see details in the dedicated section above) translates into changes of the DNA-histone core contacts and the lower end of the H3 and H3' α2 helices. Indeed, S-sulfenylation induces the apparition of denser communication hubs at the beginning of H3' α2 helix (H3'A87, H3'M89 and H3'A90 see Figure 3-b), which also strengthens the interaction prevalence of H3'Q85 (+23%) and H3'S86 (+12%). On the other side of the NCP, communication pathways in the H3α2 bearing the S-sulfenylated site are weakened, which is accompanied by a strong loss of interaction prevalence of H3S86 (-31%), which is nevertheless counter-balanced by an increased prevalence of the vicinal H3F84 (+27%).

Compared to S-sulfenylation, S-nitrosylation induces much less shifts in the canonical interaction prevalences - see Figures 4-b and S11. In line with the difference of DNA flexibility profiles (see Figure 2), the interaction prevalence of the DNA residues at the dyad is higher in the S-nitrosylated system than for S-sulfenylation, which is also the case for histone residues near SHL0.5. Some deviations are also noted in the area near H3α2 helix lower end, denoting a differential perturbation of the long-range communication pathways. For instance, the shift of interaction prevalence for H3S86 is positive with S-nitrosylation (+10%) and negative with S-sulfenylation (-31%). In the H3α1 helix,

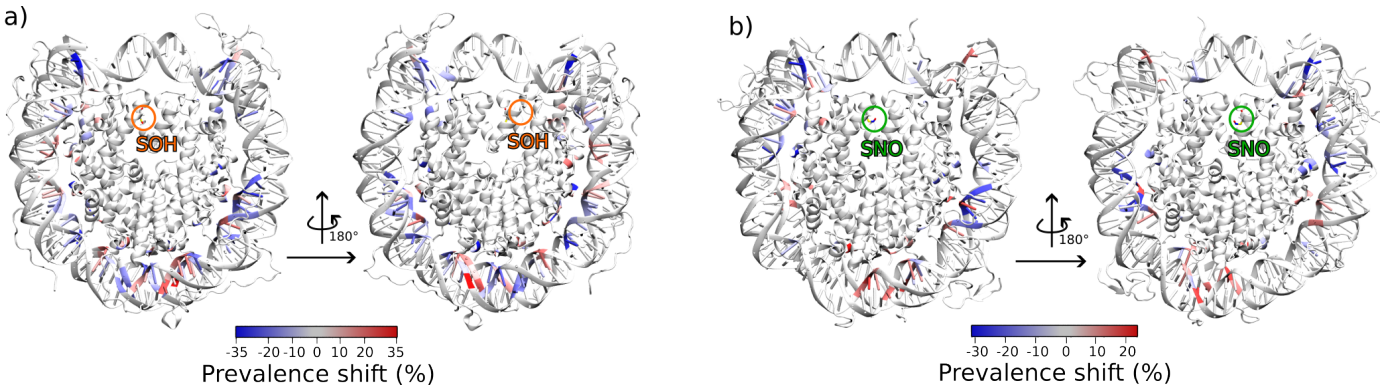

Fig. 4 Projection of the per residue DNA-histone interaction prevalence shift for a) the S-sulfenylated and b) the S-nitrosylated systems with respect to the control. Negative to positive shifts in DNA-histone interactions are depicted from blue to red. For sake of clarity, only shifts higher than 10% of prevalence are projected. Histone tails were excluded from the analysis. For each residue, the value displayed is the difference of prevalence to be involved in DNA-histone contacts between the modified system and the control one. The modified residues (SOH and SNO) are marked by orange and green circles, respectively.

H3K64 interactions with DNA are weakened with S-nitrosylation (-32%) while strengthened with S-sulfenylation (+15%), which is also the case for H3R636 (-18% with S-nitrosylation and +21% with S-sulfenylation).

A binding pocket is located near H3C110 and oxidative modifications do not influence its properties

S-sulfenylation and S-nitrosylation can behave as intermediates towards the formation of S-glutathionylated cysteines. Indeed, they allow to activate the cysteine, which can then react with glutathione. In the nucleosome, H3C110 has been shown to undergo S-glutathionylation. However, the highly buried character of this cysteine raises questions about the molecular mechanisms promoting the formation of its bulky S-glutathionylated derivative. In order to bring insights into the effect of S-sulfenylation and S-nitrosylation on the cysteine accessibility and the formation of binding pockets in its surroundings, we performed MDpocket analyses on the MD ensembles of 1KX5 (control), 1KX5+SOH (sulfenylation) and 1KX5+SNO (nitrosylation).

The canonical system already exhibits a binding pocket near the H3C110 on both NCP sides (i.e., and symmetrically near H3'C110), mainly formed by residues H3L109, H3'L126, H3H113, H3L112, H3'K122 and H3'R129. While this could be the binding site for pre-reactive complexes of activated glutathione with H3C110 (e.g. GSNO [17]), hydrophobic residues (H3/H3'L109 and H3'/H3L126) still shield the cysteine, which remains hardly accessible. Of note, GSNO, which is a putative reactant towards S-glutathionylation, harbors negative charges on its termini which could interact favorably with the positively charged residue of the binding pocket near H3C110.

These symmetrical binding pockets are retrieved from the simulations with S-sulfenylation and S-nitrosylation, which only differ by the contribution of H3'R145 to the pocket, which exhibits a mildly larger volume - see Figure 5-b. However, the oxidative modifications do not allow the modulation of the pocket shape to reach the cysteine for pre-reactive states precluding S-glutathionylation. The H3L09 adjacent to the modified cysteine

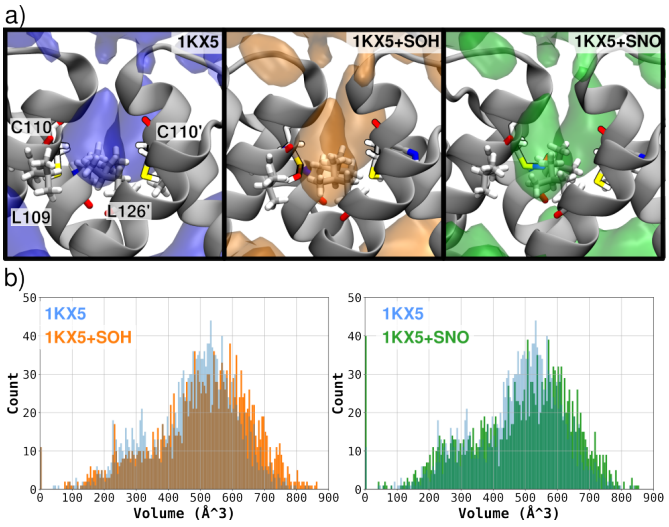

Fig. 5 a) Representation of the pockets characterized in the vicinity of H3C110, in MD ensembles from the control system (1KX5, blue, left), with S-sulfenylation (1KX5+SOH, orange, center), and with S-nitrosylation (1KX5+SNO, green, right). The hydrophobic residues shielding H3C110 and H3'C110 (L109 and L126 of each H3 copy) are depicted in licorice, as well as the two cysteines. b) Distribution of volume of the pockets near H3C110 and H3'C110 for control (in blue), S-sulfenylated systems (in orange, left) and S-nitrosylation systems (in green, right).

and the facing H3'L126 remains stable and hinder any exposure of the reactive sulfur. A slight increase in the polarity and the charge scores of the pockets is observed in the oxidized system, concomitant with a mild decrease of hydrophobicity, which might render the binding site more favorable to glutathione and its derivatives - see Figure S1. Noteworthy, the pockets characterized on the overall NCP surface in the control system remain mostly unchanged upon S-sulfenylation and S-nitrosylation -see Figure S1.

While the two H3C110 oxidative modifications used in this study do not promote the accessibility of the cysteine in our simulations, one can not rule out the possibility of an exposure of the reactive sulfur induced by the binding with the glutathione

derivative itself. The symmetrical pockets observed in the vicinity of H3C110 and H3'C110 might constitute a binding site for glutathione or its oxidized derivatives that could be the first step towards S-glutathionylation. Investigations of the interactions between glutathione and the NCP will be the topic of future investigations.

Conclusions

Histone post-translational modifications are major regulator of the chromatin dynamics. They modulate the structure and dynamics of the nucleosome through fine tune mechanisms that impact DNA compaction in a specific way. Here, we brought out new information about the impact of two oxidative histone H3C110 modifications, S-sulfenylation and S-nitrosylation, on a nucleosome core particle dynamics. Our micro-seconds timescales MD simulations provide an all-atom description of the structural signature of these two PTMs, revealing that the chemical nature of the modification drives its effect on the NCP structure. While S-sulfenylation destabilizes the DNA at the dyad and the DNA-histone interaction network, S-nitrosylation induces a milder perturbation of the NCP architecture, with essentially a destabilization of the DNA entry/exit point. We highlight allosteric effects driven by the modifications, that are transmitted through rewired communication pathways especially in H3 and H3' α2 helices. Importantly, the structural signature of S-sulfenylation in the NCP exhibits similar trends as H3C110 S-sulfonylation which we described in a previous work[19]. Overall, these results suggest a differential effect of H3C110 oxidative PTM in the nucleosome depending on their chemistry: consecutive oxidation levels of the cysteine (S-sulfenylation/S-sulfonylation) might promote remodeling events involving destabilization of the dyad (DNA sliding, NCP disassembly), while nitrosative modification (S-nitrosylation) could specifically favor DNA unwrapping.

Our results also reveal the presence of a binding pocket near H3C110/H3'C110, which could be the docking site for pre-reactive conformations prior to the non-enzymatic formation of cysteine PTM. These results bring important information as H3C110 is known to undergo bulky modifications (S-glutathionylation), whose mechanisms of formation remain unknown especially when the target cysteine is highly buried in the H3-H3' bundle. As S-glutathionylation can be formed from glutathione and an oxidized form of H3/H3'C110, we probed the effect of H3C110 S-sulfenylation and S-nitrosylation on the binding pockets properties. We show that these modifications only mildly impact the pocket near H3/H3'C110, yet they induce a slight increase of their volume and polar/charged score. This suggests that the accessibility of the cysteine might mostly be induced by the binding of a reactant (e.g., glutathione or its derivatives).

Overall, we provide here the first insights into the modulation of the NCP structure by histone oxidative PTMs, underlining their allosteric modulation of DNA flexibility, histone core intrinsic communication pathways and DNA-histone contact map. Experimental data would be a great importance to validate and fully understand how this PTM-induced re-organization of the nucleosome core particle can impact higher-order structures such as chromatin.

Author Contributions

Conceptualization and Project Administration: E. B.; Methodology and Resources: E.B., Y.K. and R.G-A; Data Curation, Visualization, Writing – Original Draft and Writing – Review & Editing: all authors.

Conflicts of interest

There are no conflicts to declare.

Acknowledgements

This work was performed using HPC resources from GENCI-IDRIS (Grant 2023-A0150714577) and EXPLOR (Grant 2019CP-MXX0983). E. B. thanks Tao Jiang and Elise Dumont for providing the flexibility analysis script.

Notes and references

1 R. K. McGinty and S. Tan, *Chemical reviews*, 2015, **115**, 2255–2273.
2 N. Gillet, E. Dumont and E. Bignon, *Biophysical Reviews*, 2024, 1–12.
3 G. Millán-Zambrano, A. Burton, A. J. Bannister and R. Schneider, *Nature Reviews Genetics*, 2022, **23**, 563–580.
4 M. Simon, J. A. North, J. C. Shimko, R. A. Forties, M. B. Ferdinand, M. Manohar, M. Zhang, R. Fishel, J. J. Ottesen and M. G. Poirier, *Proceedings of the National Academy of Sciences*, 2011, **108**, 12711–12716.
5 S. Rizza and G. Filomeni, *Biochemical Journal*, 2020, **477**, 3649–3672.
6 D. T. Hess, A. Matsumoto, S.-O. Kim, H. E. Marshall and J. S. Stamler, *Nature reviews Molecular cell biology*, 2005, **6**, 150–166.
7 D. Seth, C. T. Stomberski, P. J. McLaughlin, R. T. Premont, K. Lundberg and J. S. Stamler, *Antioxidants & Redox Signaling*, 2023, **39**, 621–634.
8 P. Anand and J. S. Stamler, *Journal of molecular medicine*, 2012, **90**, 233–244.
9 H.-L. Zhou, Z. W. Grimmett, N. M. Venetos, C. T. Stomberski, Z. Qian, P. J. McLaughlin, P. K. Bansal, R. Zhang, J. D. Reynolds, R. T. Premont *et al.*, *Cell*, 2023, **186**, 5812–5825.
10 G. Roos and J. Messens, *Free Radical Biology and Medicine*, 2011, **51**, 314–326.
11 A. E. Beedle, S. Lynham and S. Garcia-Manyes, *Nature communications*, 2016, **7**, 12490.
12 Y. Song, Z. Xu, Q. Zhong, R. Zhang, X. Sun and G. Chen, *Frontiers in Pharmacology*, 2023, **14**, 1303465.
13 C.-Y. Yang, C.-F. Yang, X.-F. Tang, L. E. Machado, J. P. Singh, W. Peti, C.-S. Chen and T.-C. Meng, *Free Radical Biology and Medicine*, 2023, **194**, 147–159.
14 Y. Ma, M. Yi, W. Wang, X. Liu, Q. Wang, C. Liu, Y. Chen and H. Deng, *Cell Death & Disease*, 2022, **13**, 944.
15 J. L. García-Giménez, C. Romá-Mateo and F. V. Pallardó, *Biofactors*, 2019, **45**, 641–650.
16 J.-L. García-Giménez, C. Garcés, C. Romá-Mateo and F. V. Pallardó, *Free Radical Biology and Medicine*, 2021, **170**, 6–18.

17 J. L. García-Giménez, G. Olaso, S. B. Hake, C. Bönisch, S. M. Wiedemann, J. Markovic, F. Dasi, A. Gimeno, C. Pérez-Quilis, O. Palacios *et al.*, *Antioxidants & redox signaling*, 2013, **19**, 1305–1320.

18 A. De Luca, N. Moroni, A. Serafino, A. Primavera, A. Pastore, J. Z. Pedersen, R. Petruzzelli, M. G. Farrace, P. Pierimarchi, G. Moroni *et al.*, *Biochemical Journal*, 2011, **440**, 175–183.

19 Y. Karami and E. Bignon, *Computational and Structural Biotechnology Journal*, 2024, **23**, 1387–1396.

20 G. A. Armeev, A. K. Gribkova, I. Pospelova, G. A. Komarova and A. K. Shaytan, *Current Opinion in Structural Biology*, 2019, **56**, 46–55.

21 G. A. Armeev, A. S. Kniazeva, G. A. Komarova, M. P. Kirpichnikov and A. K. Shaytan, *Nature communications*, 2021, **12**, 2387.

22 E. A. Morrison, L. Baweja, M. G. Poirier, J. Wereszczynski and C. A. Musselman, *Nucleic acids research*, 2021, **49**, 4750–4767.

23 M. A. Öztürk, M. De, V. Cojocaru and R. C. Wade, *Annual review of physical chemistry*, 2020, **71**, 101–119.

24 J. Huertas and V. Cojocaru, *Journal of molecular biology*, 2021, **433**, 166744.

25 Y. Peng, D. Espiritu, S. Li, D. Landsman and A. Panchenko, *Biophysical Journal*, 2022, **121**, 361a.

26 W. Humphrey, A. Dalke and K. Schulten, *J. Mol. Graph.*, 1996, **14**, 33–38.

27 Schrödinger, LLC.

28 C. A. Davey, D. F. Sargent, K. Luger, A. W. Maeder and T. J. Richmond, *Journal of molecular biology*, 2002, **319**, 1097–1113.

29 J. A. Maier, C. Martinez, K. Kasavajhala, L. Wickstrom, K. E. Hauser and C. Simmerling, *Journal of chemical theory and computation*, 2015, **11**, 3696–3713.

30 I. Ivani, P. D. Dans, A. Noy, A. Perez, I. Faustino, A. Hospital, J. Walther, P. Andrio, R. Goni, A. Balaceanu, G. Portella, F. Battistini, J. L. Gelpí, C. González, M. Vendruscolo, C. A. Laughton, S. A. Harris, D. A. Case, and M. Orozco, *Nature Methods*, 2016, **38**, 55–58.

31 J. Yoo and A. Aksimentiev, *Physical Chemistry Chemical Physics*, 2018, **20**, 8432–8449.

32 S. Han, *Biochemical and biophysical research communications*, 2008, **377**, 612–616.

33 C. W. Hopkins, S. Le Grand, R. C. Walker and A. E. Roitberg, *Journal of Chemical Theory and Computation*, 2015, **11**, 1864–1874.

34 C. Balusek, H. Hwang, C. H. Lau, K. Lundquist, A. Hazel, A. Pavlova, D. L. Lynch, P. H. Reggio, Y. Wang and J. C. Gumbart, *Journal of chemical theory and computation*, 2019, **15**, 4673–4686.

35 T. Darden, D. York and L. Pedersen, *The Journal of chemical physics*, 1993, **98**, 10089–10092.

36 E. Bignon, N. Gillet, T. Jiang, C. Morell and E. Dumont, *The Journal of Physical Chemistry Letters*, 2021, **12**, 6014–6019.

37 E. Bignon, V. E. Claerbout, T. Jiang, C. Morell, N. Gillet and E. Dumont, *Scientific reports*, 2020, **10**, 17314.

38 R. Lavery, M. Moakher, J. H. Maddocks, D. Petkeviciute and K. Zakrzewska, *Nucleic Acids Research*, 2009, **37**, 5917–5929.

39 C. Bouysset and S. Fiorucci, *Journal of Cheminformatics*, 2021, **13**, 72.

40 P. Schmidtke, V. Le Guilloux, J. Maupetit and P. Tuffi¿ 1/2ry, *Nucleic acids research*, 2010, **38**, W582–W589.

41 Y. Karami, T. Bitard-Feildel, E. Laine and A. Carbone, *Scientific reports*, 2018, **8**, 16126.

42 Y. Karami, E. Laine and A. Carbone, *BMC Bioinformatics*, 2016, **17 Suppl 2**, 13.

43 H. Kono and H. Ishida, *Current Opinion in Structural Biology*, 2020, **64**, 119–125.

44 O. Ordu, A. Lusser and N. H. Dekker, *Biophysical reviews*, 2016, **8**, 33–49.

45 S. Bilokapic, M. Strauss and M. Halic, *Nature structural & molecular biology*, 2018, **25**, 101–108.

46 S. Morioka, T. Oishi, S. Hatazawa, T. Kakuta, T. Ogoshi, K. Umeda, N. Kodera, H. Kurumizaka and M. Shibata, *Nano Letters*, 2024.